HHS Public Access

Author manuscript

Nat Microbiol. Author manuscript; available in PMC 2017 August 31.

Published in final edited form as:

Nat Microbiol. ; 2: 16226. doi:10.1038/nmicrobiol.2016.226.

A Mouse Model for MERS Coronavirus Induced Acute Respiratory Distress Syndrome

Adam S. Cockrell[a,π], **Boyd L. Yount**[a], **Trevor Scobey**[a], **Kara Jensen**[a], **Madeline Douglas**[a], **Anne Beall**[a], **Xian-Chun Tang**[d,e], **Wayne A. Marasco**[d,e], **Mark T. Heise**[b,c,¶,π], and **Ralph S. Baric**[a,b,¶,π]

[a]Department of Epidemiology, University of North Carolina-Chapel Hill, Chapel Hill, North Carolina, USA

[b]Department of Microbiology and Immunology, University of North Carolina-Chapel Hill, Chapel Hill, North Carolina, USA

[c]Department of Genetics, University of North Carolina-Chapel Hill, Chapel Hill, North Carolina, USA

[d]Department of Cancer Immunology and AIDS, Dana-Farber Cancer Institute, Harvard Medical School, Boston, MA, USA

[e]Department of Medicine, Harvard Medical School, Boston, MA, USA

Introductory Paragraph

Middle East respiratory syndrome coronavirus (MERS-CoV) is a novel virus that emerged in 2012, causing acute respiratory distress syndrome (ARDS), severe pneumonia-like symptoms, and multi-organ failure, with a case fatality rate of ~36%. Limited clinical studies indicate that humans infected with MERS-CoV exhibited pathology consistent with late stages of ARDS, which is reminiscent of disease observed in patients infected with SARS coronavirus. Models of MERS-CoV-induced severe respiratory disease have been difficult to achieve, and small animal models traditionally used to investigate viral pathogenesis (mouse, hamster, guinea pig, and ferret) are naturally resistant to MERS-CoV. Therefore, we used CRISPR/Cas9 to modify the mouse genome to encode two human amino acids (288 and 330) in the dipeptidyl peptidase 4 receptor, making mice susceptible to MERS-CoV replication. Serial MERS-CoV passage in these engineered mice was then used to generate a mouse-adapted virus that replicated efficiently within the lungs, and evoked symptoms indicative of severe acute respiratory distress syndrome (ARDS), including decreased survival, extreme weight loss, decreased pulmonary function, pulmonary hemorrhage,

[π]Corresponding authors, Correspondence and request for materials should be addressed to Dr. Ralph Baric, rbaric@email.unc.edu.
[¶]Senior authors

Author Contributions

A.S.C. conceived/designed, coordinated and executed experiments, analyzed data and wrote the manuscript. B.L.Y. developed and recovered infectious clone viruses; T.S. completed mouse experiments; K.J. designed and completed immunological experiments; M.D. helped establish and maintain mouse colony and perform molecular analysis; A.B. helped complete mouse experiments; and, X-C. T. and W.A.M. provided critical monoclonal antibody reagents. M.T.H. and R.S.B. conceived/designed experiments and wrote manuscript.

Competing Financial Interests

The authors declare no competing financial interests.

and pathological signs indicative of end stage lung disease. Importantly, therapeutic countermeasures comprising MERS-CoV neutralizing antibody treatment or a MERS-CoV spike protein vaccine protected engineered mice against MERS-CoV-induced ARDS.

The severity of respiratory illness caused by MERS-CoV, its pandemic potential through human-to-human respiratory transmission, and a dearth of effective treatments necessitates the development of new MERS-CoV therapies and vaccines. Effective vaccine and therapeutic development requires preclinical animal models that resemble the pathogenesis of human MERS-CoV infection. Additionally, these models should: i) include a measure of mortality associated with severe respiratory disease; ii) not be confounded by neurological complications due to high viral loads in the brain; iii) exhibit sustained, high level viral replication within the lungs of infected animals; iv) exhibit lung pathology associated with human ARDS; v) maintain innate expression of the MERS-CoV host receptor, dipeptidyl peptidase 4 (DPP4) to prevent perturbation of immunological homeostasis; vi) be genetically tractable to study host genes that regulate responses to MERS-CoV vaccines and therapeutics; and vii) exhibit reproducibility.

Conventional non-human primate (NHP) models have been established for MERS-CoV in both the rhesus macaque and common marmoset[1–4]. NHPs are instrumental for the preclinical development of therapeutics, however, these models are cost prohibitive for initial screening of large numbers of vaccine and therapeutic candidates, challenging to work with for routine pathogenesis studies, limited in availability and typically require high viral challenge doses into multiple sites. Furthermore, two recent studies contradict the initial studies in NHPs, which may complicate use of either the rhesus macaque[5] or the common marmoset[6] models for routine vaccine or therapeutic testing.

MERS-CoV fails to replicate in traditional small animal models (mouse, hamster, guinea pig, and ferrets), due to the inability of the receptor binding domain (RBD) in the MERS-CoV spike protein to interact with the respective DPP4 receptor[7–10]. In addition to acting as the MERS-CoV receptor, DPP4 regulates T cell activation, cytokine function, and trans-endothelial migration to sites of inflammation[11]. Therefore, overexpression of DPP4 may result in immune dysregulation. Effective models would therefore, ideally promote functional MERS-CoV/DPP4 interactions, with minimal perturbations of innate DPP4 expression, signaling activity, or tissue distribution. Classic strategies to overcome receptor incompatibilities to generate susceptible mice have relied on generalized or tissue-specific transgenic over-expression approaches to drive expression of the human receptor (hDPP4) in the mouse[12–15]. Although MERS-CoV can elicit respiratory disease in hDPP4 overexpression models, these models exhibit a fatal CNS and systemic multi-organ disease[12–14], likely due to non-specific overexpression of receptor throughout the animal, which complicates the study of MERS-CoV-induced respiratory pathogenesis in these models.

In this manuscript, we leveraged our knowledge of which determinants allow mouse DPP4 to act as a functional MERS-CoV receptor[7] by using CRISPR/Cas9 genome editing technology to insert human codons at positions 288 and 330 in the mouse DPP4 gene. This strategy resulted in a mouse that is permissive for MERS-CoV infection, while maximally

preserving the species-specific interaction networks critical for DPP4 immune function. Generation of mice carrying a chimeric mDPP4 molecule (A288L/T330R), combined with a mouse adapted strain of MERS-CoV, allowed us to generate a mouse model that resembles severe MERS-CoV-induced respiratory disease without bystander neurologic disease. In parallel, we demonstrate that this model system can be used for the development and testing of MERS-CoV vaccines and therapeutics.

Results

A CRISPR/Cas9 generated mouse model for MERS-CoV infection

We had previously demonstrated that the introduction of two human amino acids at positions 288 and 330 in the mouse DPP4 (mDPP4) receptor can support MERS-CoV docking, entry, and replication in cell culture[7]. These determinants are located at exons 10 and 11 of mDPP4 on chromosome 2 (Fig. 1a and Supplemental Fig. 1). Therefore, we used CRISPR/Cas9 genome editing to concomitantly introduce these determinants (A288L and T330R) into the mouse DPP4 receptor (Fig. 1a and Supplemental Table 1). Two lines of C57Bl/6J-derived mice were generated that were either homozygous (288-330$^{+/+}$) or heterozygous (288-330$^{+/-}$) for the chimeric mDPP4 alleles (Fig. 1a). The 288-330$^{+/+}$ homozygous mice encode the 288L and 330R changes on both chromosomes, thereby only expressing mDPP4 with both changes (Fig. 1a). The 288-330$^{+/-}$ heterozygous mice encode the 288L and 330R changes on one chromosome and the C57Bl/6J wild-type amino acids, A288 and T330, on the other chromosome, thereby expressing both mutated and wild-type mDPP4 (Fig. 1a). The innate mDPP4 expression levels and patterns in the lungs, kidneys, and brains of 288-330$^{+/+}$ and 288-330$^{+/-}$ mice reflect those observed in C57Bl/6J wild-type mice (Fig. 1b and 1c; Supplemental Fig. 2). Dipeptidyl peptidase 4 is central to the maintenance of glucose homeostasis in mammals[16]. Blood glucose levels are within the normal range observed in C57Bl/6J wild-type mice, supporting the hypothesis that biological mDPP4 functions were not altered in 288-330$^{+/+}$ and 288-330$^{+/-}$ mice (Supplemental Fig. 2). Moreover, basal CD4+ T cell expression of IL-2, TNF-α, IFN-γ, CD69, CD25 and mDPP4 (CD26) from the 288-330$^{+/+}$ and 288-330$^{+/-}$ lines was comparable to the levels observed in C57Bl/6J wild-type mice (Supplemental Fig. 3). Notwithstanding functional T cell assessment, these results suggest that minimal alteration of the 288 and 330 alleles does not alter basal T cell activation status. Overall expression levels, expression patterns, biological function, and immunological profiles of mDPP4 are comparable to those of C57Bl/6J wild-type mice following site-specific modification of the 288 and 330 alleles.

The 288-330$^{+/+}$ and 288-330$^{+/-}$ mice support efficient infection and replication of the human MERS-CoV strain HCoV-EMC/2012, the camel MERS strain Dromedary/Al-Hasa-KFU-HKU13/2013, and a recombinant virus derived from a molecular infectious clone (icMERS), in the lungs, but these virus strains could not replicate in C57Bl/6J wild-type mice that retain the original murine A288 and T330 alleles (Fig. 1d). In parallel, a MERS-CoV tissue-culture adapted variant derived by infection of NIH3T3 cells ectopically expressing the chimeric mDPP4 (A288L/T330R) receptor, was found to encode a 3 amino acid insertion and a single amino acid change (RMRL) in the S2 region of the spike gene. MERS-0, a recombinantly derived virus encoding the RMRL S2 mutations, demonstrated significantly enhanced

replication both in cell culture (Supplemental Fig. 4) and in the lungs of 288-330$^{+/+}$ and 288-330$^{+/-}$ mice (Fig. 1d). Despite replicating to significantly higher virus titers *in vivo* than the other isolates, MERS-0 exhibited no evidence of severe clinical disease symptoms (Supplemental Fig. 4). Lung histology demonstrated that nucleocapsid antigen from MERS-0, and the other strains, was readily detected in the lungs of infected mice by immunohistochemistry, but infected lungs exhibited only moderate signs of respiratory pathology and inflammation (Fig. 1e). These results demonstrated that we developed a MERS-CoV model that can support high levels of viral replication through day 3 post-infection, but required further *in vivo* adaptation to achieve respiratory symptoms characteristic of MERS-CoV infection in humans.

Mouse adaptation of MERS-CoV induces ARDS-like severe respiratory disease

The recombinantly-derived MERS-0 virus was then mouse adapted by serial passage for 15 rounds through the lungs in 288-330$^{+/-}$ mice at 3 day intervals, resulting in the MERS-15 strain. Infection of 288-330$^{+/+}$ mice via the intranasal (IN) route with MERS-15 resulted in ~70% mortality (genuine mortality, rather than mice meeting the typical 20% weight loss cutoffs associated with human euthanasia criteria), while 100% of infected 288-330$^{+/-}$ mice survived (Fig. 2a). Nonetheless, both lines exhibited 20–25% weight loss by day 6 post-infection, in contrast to MERS-0 infected 288-330$^{+/+}$ mice or MERS-15 infected C57Bl/6J wt mice which exhibited no weight loss (Fig. 2b). Significantly higher levels of MERS-15 replication was detectable in the lungs of both 288-330$^{+/+}$ and 288-330 $^{+/-}$ mice at days 3 and 6 post-infection, while MERS-0 was mostly cleared from the lungs by day 6 post-infection (Fig. 2c and 2d). Similar to MER-0, MERS-15 could did not replicate in wild type C57Bl/6 mice. Importantly, the observed decreases in survival and weight loss induced by MERS-15 were not confounded by neurological complications from brain infection, as plaque assays for replication competent virus and RT-PCR at days 3 and 6 post-infection were negative (Supplemental Fig. 5). Moreover, qRT-PCR on the same samples demonstrated >10^6 increase in detectable viral transcripts in infected lungs compared to similarly infected C57Bl/6J mice, with no detectable viral transcripts in the brains of these mice.

Although mortality and weight loss provide important measures of MERS-CoV-induced disease, these parameters do not directly assess the impact of viral replication on respiratory function. Therefore, to directly assess the impact of MERS-15 infection on respiratory function in 288-330$^{+/+}$ or 288-330$^{+/-}$ mice, we measured respiratory function using unrestrained plethysmography, as previously demonstrated for respiratory pathogenesis in mouse models of SARS and influenza[17]. MERS-15 elicited severe lung disease as quantified by Penh (enhanced pause), a unit-less measure that reflects airway obstruction/restriction due to debris in the airway, and EF50 (mid-tidal expiratory flow), which represents the flow rate at which 50% of the tidal volume has been expelled, in a single breath[17]. MERS-15 infection led to significant increases in both Penh and EF50 in 288-330$^{+/+}$ and 288-330$^{+/-}$ mice through day 6 post-infection, compared to 288-330$^{+/+}$ mice infected with MERS-0 and C57Bl/6J wt mice infected with MERS-15 (Fig. 3a & 3b), demonstrating that MERS-15 elicits severe respiratory distress in mice carrying the chimeric DPP4 receptor. This was further supported by our observation of severe hemorrhage in lungs from both 288-330$^{+/+}$

and 288-330$^{+/-}$ mice infected with MERS-15 at days 3 and 6 (Supplemental Fig. 6), inflammatory infiltrates by day 3 (Fig. 3c), and respiratory pathology associated with severe acute respiratory distress, including hyaline membrane formation, intraalveolar edema, perivascular cuffing, and severe inflammation, at day 6 post-infection (Fig. 3d). Quantitative comparison of the lung pathology in 288-330$^{+/+}$ mice infected with MERS-15 and MERS-0 demonstrates that MERS-15 induces significant levels of pathology commensurate with ARDS by day 6 post-infection (Supplemental Fig. 7). Although we have not conducted an exhaustive assessment of every extra-pulmonary tissues in the 288-330$^{+/+}$ mice, we could not detect viral replication in the brain even at doses of 5×10^6 PFU through day 6 when the humane euthanasia endpoints were reached, and the pathology observed in our model is consistent with severe respiratory pathology associated with fatal ARDS in the only published case study of a human MERS-CoV infection[18].

Identification of MERS-CoV adapted mutations associated with severe respiratory disease

We anticipated that the MERS-CoV genome would acquire mutations due to immunological pressure, and/or enhanced virus fitness, during mouse adaptation. Two viral clones, MERS-15 clone 1 (MERS-15 C1) and MERS-15 clone 2 (MERS-15 C2) were isolated by plaque purification from the MERS-15 heterogeneous virus population. MERS-15 C2 showed increased mortality (Fig. 4a) and significantly increased hemorrhage through day 6 post-infection (Supplemental Fig. 8), whereas both clonal isolates showed 25–30% weight loss (Fig. 4b) and high levels of virus replication through day 6 post-infection when humane euthanasia endpoints were reached (Fig. 4c). The lung pathology elicited by MERS-15 C2 resembled that obtained with the primary MERS-15 virus (Fig. 4d), demonstrating similar pathologies including edema, hyaline membrane formation, and perivascular cuffing. Sequencing of the entire MERS-15 C2 genome revealed a set of unique missense mutations, acquired during *in vivo* passaging, in nsP2, nsP6, and nsP8, and a large deletion in Orf4b that may be responsible for the enhanced disease observed with MERS-15 (Supplemental Fig. 9). Sequencing of MERS-15 C1 revealed some differences that may influence the capacity of the virus to elicit the increased mortality observed with MERS-15 C2, namely mutations in nsP2 and an expanded deletion that extends from Orf4b into Orf5 (Supplemental Fig. 9). Moreover, 5′-RACE revealed that the nucleotide at position 2 of the 5′ UTR is deleted in both clones (Supplemental Fig. 9). Generation of an infectious clone harboring all of the MERS-15 C2 mutations (icMERSma1) demonstrated that disease could be recapitulated with an infectious dose of 5×10^6 PFU (Supplemental Fig. 10). Decreasing the dose by 10-fold to 5×10^5 PFU resulted in weight loss that paralleled what is observed with 5×10^6 PFU, however the 5×10^5 PFU dose exhibited a slight decrease in mortality through day 7 post-infection (Supplemental Fig. 10). Although additional studies will be needed, comparative genomic analysis of clones 1 and 2 indicates that nsP2 and Orf5 may have a significant role in determining disease outcome. Therefore, the MERS-15 C2 derived virus, combined with the 288-330$^{+/+}$ mouse line, represent useful tools for studying MERS-CoV pathogenesis or assessing therapeutic countermeasures against MERS-CoV-induced ARDS.

3B11, human monoclonal antibody, protects from MERS-CoV elicited severe respiratory disease

Human monoclonal antibodies (hmAB) provide a robust strategy for the treatment of newly emerged viruses in humans. HmAB 3B11 is a human antibody that targets the RBD of the MERS-CoV spike protein[19], which is effective in non-human primates[5]. Since the MERS-15 C2 adapted virus acquired no RBD mutations (Supplemental Fig. 9), we reasoned that 3B11 hmAb should protect 288-330$^{+/+}$ mice from MER-15 C2 challenge. As hypothesized, pre-treating mice for 12 hours with 3B11 provided 100% protection against MERS-15 C2 challenge (Fig. 5a & 5b). Moreover, 3B11 treatment reduced viral loads in the lungs of infected mice to undetectable levels (Fig. 5c and Supplemental Fig. 11), and protected from loss of respiratory function (Fig. 5d) (Supplemental Fig. 11), pulmonary hemorrhage (Supplemental Fig. 11) and severe pathological changes (Supplemental Fig. 12). In contrast, pretreatment with isotype control antibody provided no protective effect. Therefore, these data convincingly demonstrate that our preclinical mouse model of severe respiratory disease and mortality, can serve as a platform for assessing MERS-CoV therapeutics.

VRP-derived spike protein vaccines protect from lethal infection

To examine vaccine efficacy in the 288-330$^{+/+}$/MERS-15 C2 model, mice were vaccinated with Venezuelan equine encephalitis replicon particles (VRPs) expressing MERS-CoV spike protein (spike-VRP), or mock vaccinated with VRPs that express GFP (GFP-VRP), boosted at 4 weeks post prime, and challenged with MERS-15 C2 at 4 weeks post-boost. All mice receiving spike-VRP survived and exhibited no weight loss following challenge, compared to GFP-VRP mock vaccinated animals (Fig. 6a and 6b). Spike-VRP vaccination significantly reduced MERS-15 C2 replication in the lungs of infected mice by both plaque titer (Fig. 6c) and by viral antigen staining (Supplemental Fig. 14), while also protecting from severe respiratory disease as assessed by Penh (Fig. 6d) and EF50 (Supplemental Fig. 13), lung hemorrhage (Supplemental Fig. 13), and pathological indications of severe acute respiratory disease (Supplemental Fig. 14). Neutralization of MERS-15 C2 with pre-challenge serum from spike-VRP vaccinated mice validated the presence of high titer neutralizing antibodies in the serum of vaccinated 288-330$^{+/+}$ mice (Supplemental Fig. 13). Our data demonstrate that the spike-VRP vaccine provokes an adaptive immune response capable of protecting mice from a lethal challenge of MERS-CoV, thereby extending the utility of our preclinical mouse model of severe respiratory disease to include vaccine evaluation.

Discussion

The MERS-CoV preclinical mouse model described here demonstrates for the first time that the CRISPR-Cas9 system can be employed to genetically edit a non-permissive host receptor to generate a susceptible model for an emerging infectious pathogen. The 288-330$^{+/+}$ MERS-CoV mouse model resembles the severe, and often fatal, respiratory distress syndrome observed in humans that can be prevented through treatment with the 3B11 neutralizing monoclonal antibody[19], or a VRP-based vaccine directed to the MERS-CoV spike protein[15,20]. Coupled with an inability to elicit escape mutants, 3B11 has also been tested in NHPs[5], making it an excellent candidate for downstream human studies.

However, existing NHP models rely on qRT-PCR, rather than measures of infectious virus, to quantify viral loads, and these models do not reproducibly result in the severe respiratory disease or mortality observed in human MERS patients[1–4]. Therefore, the results from our model complements the NHP 3B11 studies by directly demonstrating that 3B11 does reduce levels of infectious MERS-CoV in the lungs, while preventing severe virus-induced respiratory pathology, loss of respiratory function, and mortality.

In fatal cases of human MERS-CoV infections, individuals exhibit severe respiratory distress requiring mechanical ventilation, and the only published human autopsy from a MERS-CoV fatality reported histopathology that included diffuse alveolar damage with denuding of bronchiolar epithelium, hyaline membrane formation, type 2 pneumocyte hyperplasia, and edema[18]. Furthermore, MERS-CoV antigen staining localized the virus to pneumocytes and syncytial cells[18]. Infection of type I and II pneumocytes can lead to cell death as observed in autopsies of patients that have died from severe respiratory infections with influenza and SARS[21,22]. Moreover, pneumocyte cell death has been proposed to cause decreased respiratory function as measured by whole body plethysmography in a mouse model of influenza[23]. Commensurate with these previous studies our MERS-CoV mouse model demonstrates wide-spread infection of pneumocytes and pathology consistent with diffuse alveolar damage and severe respiratory disease. This is corroborated with decreased pulmonary function in the MERS-CoV model, as measured by plethysmography, which may be associated with widespread infection, and possibly death of pneumocytes and airway epithelial cells. Therefore, this model system provides the field with the opportunity to investigate the mechanisms that lead to MERS-CoV-induced pathology and severe respiratory disease, in the absence of any CNS complications.

Other MERS-CoV mouse models have employed the more traditional method of expressing the full-length human DPP4 receptor to facilitate MERS-CoV infection[12–15,24]. These models exhibited infection/replication in the lungs following intranasal administration at low viral doses (10^2–10^5 PFU), which in some cases resulted in pathology indicative of pneumonia-like disease[12–14]. One limitation of 288-330$^{+/+}$ MERS-CoV model described here is the use of high viral loads to achieve severe, and often, fatal respiratory disease. Further adaptation may afford the use of lower infectious doses that would allow for a model of mild disease with subsequent recovery at later time points, as has been described with SARS-CoV[25]. In this context, it is interesting that the deletion of MERS-CoV ORF4b, a phosphodiesterase and antagonist of RNAseL activity in human cells, appeared less critical for eliciting severe disease in rodents[26], suggesting possible species specific modes of action *in vivo*. Deletions in some SARS-CoV interferon antagonist genes and accessory ORFs have also yielded subtle changes in overall virulence *in vivo* as well[27,28]. However, it is also important to point out that balance must be achieved between the virulence of mouse adapted virus, which enhances the model's capacity to replicate human disease phenotypes, and the number of mutations required to significantly reduce the LD50 dose.

Conventional models employing constitutive overexpression of hDPP4 MERS-CoV receptor demonstrate widespread infection of extra-pulmonary tissues including brain, kidney, liver, spleen and heart[12–14], and two of these studies indicated that the mice exhibit multi-organ failure[13,14]. Furthermore, high viral loads were detected in the brains of mice in all

transgenic hDPP4 overexpression models[12–14]. Importantly, Li et al. concluded that "mortality correlated with brain infection, suggesting that infection of this organ was most important for the high mortality observed in K18-hDPP4 mice"[13]. While these lethal models have value for vaccine and immunotherapeutic testing[29], small molecule inhibitors that are effective in the lung may be limited in their efficacy due to an inability to cross the blood brain barrier[30]. Similar neurologic complications were observed in model systems for SARS that used over-expression, or tissue-specific constitutive promoters, to express human angiotensin 1 converting enzyme 2 (ACE2) in mice[31]. While additional human pathology studies are needed to determine the extent of extra-pulmonary sites of MERS-CoV replication and their impact on MERS-CoV disease, it is clear that respiratory replication and pathology is an important aspect of human MERS-CoV disease. Therefore, an important attribute of the 288-330$^{+/+}$ model is that the lack of detectable viral replication in the CNS means that this model can be used to study MERS-CoV-induced pulmonary disease without the confounding effects of death due to CNS infection.

Recently, a debate has emerged around the safety of performing GOF studies with highly pathogenic viruses (MERS-CoV, SARS-CoV, Influeza H5N1, etc.) (http://www.gryphonscientific.com/gain-of-function/). As demonstrated here, GOF studies were absolutely necessary to develop a mouse model that reflects ARDS pathology previously observed in humans infected with respiratory pathogens. Importantly, the GOF studies performed here yielded MERS-CoV strains that reflect the complexity of clinical isolates recently identified in humans, wherein deletions were identified in Orf3 and Orf4a[32]. Moreover, these GOF studies have allowed us to identify mutations in MERS-CoV proteins that may influence how MERS-CoV interacts with, and possibly circumvents, host immune responses. Nevertheless, future studies to evaluate host factors that contribute to MERS-CoV disease will be constrained in this model, as well as hDPP4 expression models, by the fact that the mice must be back-crossed to mouse lines harboring modified endogenous genes (e.g. knock-out mice). This limitation may be overcome through additional GOF studies that facilitate MERS-CoV adaptation to the innate mouse DPP4 receptor molecule. The continued threats from novel emerging pathogens (e.g. Zika virus) will command the rapid development of physiologically relevant animal models to evaluate therapeutic countermeasures, thereby necessitating viral adaptation to host immunity to achieve effective models. It is critical that the GOF regulatory structure not impede the development of robust animal models of human disease, which are essential for protecting the public health.

Methods

Viruses, cells, and plaque assays

All virus stocks were prepared on Vero CCL81 cells (ATCC, Manassas, VA). Vero CCL81 cells were routinely maintained in Dulbecco's modified Eagle's medium (DMEM) (Gibco, Carlsbad, CA) supplemented with 10% fetal bovine serum (FBS) (Sigma, F2442) and 1X antibiotic/antimycotic (Gibco, Carlsbad, CA). All viruses were harvested in OptiMEM media (Gibco, Carlsbad, CA) supplemented with 3% FBS, 1X antibiotic/antimycotic, 1X nonessential amino acids (Gibco, Carlsbad, CA), and 1X sodium pyruvate (Gibco, Carlsbad, CA). The wild-type EMC2012 strain of MERS-CoV was used at passage 10 (originally

provided by Bart Haagmans at passage 8), infectious clone MERS (icMERS) was previously generated by the Baric lab[33], MERS camel strain Dromedary/Al-Hasa-KFU-HKU13/2013 was used at passage 5 and was provided at passage 4 by Malik Peiris (University of Hong Kong, China), and MERS-0 was generated by the Baric lab as described below. Virus titers were determined by plaque assays on Vero CCL81 cells[33]. All viruses were maintained under biosafety level (BSL)3 conditions with redundant fans and personnel powered-air purifying respirators (PAPRs), scrubs, Tyvek suits, Tyvek aprons, and double layers of gloves.

An icMERS-tRFP virus[33] was passaged for 10 rounds on NIH3T3 cells (ATCC, Manassas, VA) that were generated to stably overexpress the mDPP4 receptor containing A288L and T330R, referred to here as 288/330 mDPP4 NIH3T3 cells. The mDPP4 A288L/T330R expression cassette used to generate the cell line was described previously[7]. Sequencing of the passaged virus identified a 3 amino acid (RMR) insertion after amino acid 884 in the spike protein and an S885L change. These changes were sub-cloned back into the MERS-CoV infectious clone by overlap PCR of the F fragment with the following primers: 5′-ggTTTCCAgAAgTgTgAgCAATTACTgCgCg-3′, 5′-gCAggCCTCTgCAgTCgACgggCCCgggATCCAATgCC-3′, 5′-CCTgTTTCTATATCTACTggCAgTCgTAgAATgCggCTTgCACgTAgTgCTATTgAggATTTgC-3′, and 5′-gCAAATCCTCAATAgCACTACgTgCAAgCCgCATTCTACgACTgCCAgTAgATATAgAAACAgg-3′. The F fragment is one part of a 7 plasmid system (A, B, C, D1, D2, E, and F) that permits partitioning of the entire genome to generate infectious MERS-CoV viruses, as described previously[33]. The PCR product encoding the insertion was sub-cloned back into the F fragment with MscI and BamHI restriction enzymes, and validated by sequencing. Recombinant MERS-0 virus was used for the *in vivo* passage experiments, which were gain-of-function (GOF) studies reviewed and approved by the National Institutes of Health (NIH). Vero-81 and NIH-3T3 cells were originally received from ATCC, which indicates that cell lines are authentic and confirms that cell lines are mycoplasma free. None of the working cell line stocks were authenticated or tested for mycoplasma recently, although the original seed stocks used to create the working stocks are free from contamination. Additionally, both cell lines are authenticated by morphological and cytopathological evaluation. Furthermore, Vero-81 cells are confirmed for DPP4 overexpression by capacity to be infected, and replicate MERS-CoV.

Generation of mice with mouse DPP4 modified at position 288 (exon 10) and 330 (exon 11)

The alleles encoding amino acids 288 and 330 are shown in Supplemental Figure 1. Genomic engineering of these alleles with the CRISPR/Cas9 genome editing system was performed at the UNC-CH Animal Models Core Facility. The mRNA encoding Cas9 endonuclease and guide RNAs (gRNAs) were based on the system established by Mali et al.[34] and prepared as described here. Guide RNAs (Supplemental Table 1) were generated through *in vitro* transcription reaction using T7 High Yield RNA Synthesis Kit (NEB #E2040S), wherein 1 μg DraI linearized template DNA was used in a 20 μl reaction following kit guidelines for short RNA transcripts. The reaction was incubated at 37°C overnight, followed by DNase I (RNase-free) digestion for 15 mins at 37°C. The gRNAs

were then purified using an RNeasy Column following guidelines for short RNA purification (Qiagen). Capped and polyadenylated Cas9 mRNA was prepared through *in vitro* transcription reaction using mMESSAGE mMACHINE T7 ULTRA KIT (Life Technologies, AM1345). Capped mRNA was generated with 1 μg hCas9-T7 linearized plasmid DNA added into a 20 μl reaction containing 1X NTP/ARCA, 1X T7 reaction buffer, and 2 μl T7 enzyme. The reaction was incubated at 37°C for 1 hour, followed by addition of 1 μl TURBO DNase and digestion at 37°C for 15 mins. To add a PolyA tail to the capped mRNA, the 20 μl reaction mix from step 1 was mixed with nuclease-free water (36 μl), 5X E-PAP Buffer (20 μl), 25 mM $MnCl_2$ (10 μl), ATP Solution (10 μl), and E-PAP (4 μl) to a final reaction volume of 100 μl. The reaction was incubated at 37°C for 30–45 mins. The capped & polyadenylated RNA was purified by LiCl precipitation and resuspended in microinjection buffer (5 mM Tris, 0.1 mM EDTA, pH 7.5).

Fertilized zygotes were collected from C57BL/6J females that had been super ovulated and mated to C57BL/6J males. Pronuclear microinjection was performed with 50 ng/μl Cas9 mRNA, 50 ng/μl guide RNA Dpp4-g59B, 25 ng/μl guide RNA Dpp4-g88B and 50 ng/μl each Dpp4-A288L-B and Dpp4-T330R-B donor oligos (Supplemental Table 1). Injected embryos were implanted into pseudopregnant recipients and resulting pups were screened for alleles encoding changes (Supplemental Fig. 1) at positions 288 and 330. Mutations at the 288 position were detected by amplifying biopsy DNA samples with the following primers: Dpp4-E10ScF1 5′-GATTCTGAGCAAGCAAACACGC-3′and Dpp4-E10ScR1 5′-CCACAAGGTATCCCACAGAGACG-3′. The 752 bp PCR product was sequenced with primer Dpp4-E10-SqR1 5′-CAAGAACCACACCAATGGAAAGTC-3′. Mutations at the 330 position were detected by amplifying biopsy DNA samples with the following primers: Dpp4-E11ScF1 5′-AAGTGCTGGGATTATAGGTGGTCAC-3′ and Dpp4-E11ScR1 5′-GTGTTTACATTCTAAGTTGGGTTTCTGC-3′. The 767 bp PCR product was sequenced with primer Dpp4-E11-SqF1 5′-GCATGTTATCCACTGTGCCATCTC-3′. Five of 66 live animals produced showed evidence of both the 288 and 330 modifications. Founders with both expected modifications were backcrossed to C57Bl/6J mice to identify animals with the 288 and 330 modifications in *cis*. F1 animals with both the 288 and 330 modifications were then intercrossed to produce homozygous breeder pairs for colony enrichment and downstream studies.

Mouse infections

Genetically engineered mice, with modified mouse DPP4 receptor, were housed and bred in accordance with guidelines established by the Department of Laboratory Animal Medicine (DLAM) at The University of North Carolina at Chapel Hill (UNC-CH). Since the 288-330$^{+/+}$ and 288-330$^{+/-}$ mice are novel mouse lines developed in the Baric lab, experiments utilized available male and female mice that ranged 12–20 weeks of age. Based on availability at the time of each experiment, experimental and control animals were age- and sex-matched. No blinding was used in any animal experiments, and animals were not randomized. Sample sizes were determined from preliminary data that would yield statistically significant differences. Mouse studies were executed under ABSL3 conditions as described previously[35]. Prior to viral infection mice were anesthetized by administering 50μl of a ketamine/xylazine mixture intraperitoneally, and then infected intranasally with a

50μl volume of virus at 5×10^6 PFU. Incomplete infections due to bubbling of inoculum from the nasal cavity, inability to inhale the entire dose, or inoculum going into the mouth were noted, and these mice were considered failures and were excluded, as done previously[35]. Following sedation and infection mice were monitored daily for weight loss and survival, as well as signs that animals were moribund (including labored breathing, lack of movement, and lack of grooming). Mice that reached 20% weight loss were placed under exception, and monitored at least twice daily. Mice that approached 30% weight loss were immediately euthanized. Mice deemed moribund were euthanized at the discretion of the researcher. Mice were euthanized with an isoflurane overdose followed by a secondary thoracotomy, at the time point indicated in results, for collecting lung tissues. In the absence of a thoracotomy, cervical dislocation was used as a secondary euthanasia method. All are approved methods of the Institutional Animal Care and Use Committee (IACUC) at The University of North Carolina at Chapel Hill.

Ethics Statement

Mouse studies were executed in accordance with the recommendations for the care and use of animals by the Office of Laboratory Animal Welfare (OLAW) at NIH. The Institutional Animal Care and Use Committee (IACUC) at UNC-CH approved the animal studies performed here (protocol, IACUC 13–272), using a ~30% weight loss for humane euthanasia. Synthetically reconstructed MERS-CoV viruses were approved by the UNC-CH Institutional Biosafety Committee (IBC), which also considered gain-of-function research concerns prior to execution of these experiments.

Analysis of Serum Glucose Levels

All blood glucose measurements were taken following a six hour fast. Blood glucose was measured via tail clip sampling using an AlphaTRAK 2 glucometer (Abbott Laboratories)[36]. This system is designed for use in laboratory mice with a normal range of 111 to 205 mg/dL (6.1 to 11.38 mmol/L) blood glucose, and a detection limit of 20 to 750 mg/dL (1.1 to 41.62 mmol/L).

Adaptation of MERS-0 in humanized mice

The recombinant virus MERS-0 was passed through the lungs of 288-330$^{+/-}$ mice every three days for 15 passages to obtain a MERS-CoV (MERS-15), adapted to cause respiratory disease in mice. At each passage the lungs were homogenized and 50μl of lung homogenate was used for intranasal infection of a naïve 288-330$^{+/-}$ mouse. The MERS-15 mouse-adapted virus was assessed for survival, weight loss, lung titer, hemorrhaging, respiratory function, and histopathology indicative of diffuse alveolar damage and acute respiratory distress syndrome. Clonal isolates of the MERS-15 virus were obtained by plaque purification, amplification on Vero CCL81 cells, and sequenced to determine mutations acquired during mouse adaptation of the virus. All sequencing was performed at the UNC-CH Genome Analysis Facility. MERS-15 clone 2 recapitulated the severe respiratory disease observed with MERS-15, therefore all subsequent experiments were performed with the plaque-purified MERS-15 clone 2.

Human monoclonal 3B11 antibody protection study

The 288-330$^{+/+}$ mice were prophylactically administered 250μg of either 3B11 human monoclonal antibody or F10 isotype control antibody by intraperitoneal injection[19] 12 hours prior to infection with MERS-15 clone 2. Mice were monitored daily for weight and survival, and sacrificed at days 3 and 6 post-infection to collect lungs for histology, viral titer by plaque assay, and evaluation of lung hemorrhaging. Respiratory function was measured at day 0 to establish a baseline and then again at days 3 and 6 post-infection. The isolation and production of the 3B11 and F10 antibodies was as previously described[19].

Spike-VRP vaccine study and Virus Neutralization Assay

The MERS-CoV gene encoding the spike protein and GFP gene were packaged into Venezuelan equine encephalitis virus (VEE) replicon particles generated with helper constructs from the 3526 attenuated strain, under BSL2 conditions, as previously demonstrated[20]. Mice were administered a prime vaccination of 10μl by footpad injection of either spike-VRP (1×10^5 PFU) or the control GFP-VRP (1×10^5 PFU). Twenty-eight days later mice were boosted with the same dose of their respective VRP strain. At 28 days post-boost, all vaccinated mice were challenged with 5×10^6 PFU of MERS-15 clone 2. Mice were monitored daily for weight and survival, and sacrificed at days 3 and 6 post-infection to collect lungs for histology, viral titer by plaque assay, and evaluation of lung hemorrhaging. Respiratory function was measured at day 0 to establish a baseline and then again at days 3 and 6 post-infection.

The presence of MERS-15 clone 2 specific serum antibodies was assessed by the plaque reduction neutralization titer assay. Pre-challenge serum samples were collected at 25 days post-boost with the Spike-VRP vaccine and the GFP-VRP mock. Virus neutralization assays were performed as described previously[35]. The percentage of plaque reduction was calculated as (1- (no. of plaques with Spike-VRP or GFP-VRP serum/no. of plaques with serum from naïve 288-330$^{+/+}$ mice)) × 100.

Respiratory Function

Respiratory function was measured for individual mice, at the indicated time points, as demonstrated previously for SARS-CoV and Influenza A virus[17]. Briefly, individual mice were acclimated for 30 minutes in individual plethysmography chambers (Buxco Systems, Wilmington, NC), and then each breath was quantitated over a 5 minute period. Mice were routinely randomized into different chambers to avoid measurement biases that could result between chambers. Data for enhanced pause (Penh) and expiratory flow rate at 50% tidal volume (EF50) were analyzed as previously described by our group[17].

Histology

Lung, brain, and kidney samples were placed in 10% phosphate buffered formalin for >7days at 4°C for fixation. Fixed tissue samples were then removed from the BSL3 placed into cassettes for embedding in paraffin, and submitted to the Lineberger Comprehensive Cancer Center Animal Histopathology Core for processing, sectioning and staining. Tissue sections (5μm) were stained for hematoxylin and eosin, and for MERS-CoV nucleocapsid antigen using mouse anti-MERS nucleocapsid serum at 1:250 dilution. The nucleocapsid

antiserum was generated in the Baric lab using MERS-CoV nucleocapsid-VRP particles in Balb/c mice as described previously[20]. Antigen was visualized using DAB staining. An Olympus DP71 camera attached to an Olympus BX41 microscope was used to capture images with 10X and 40X objectives. Histopathology was scored, blinded to infection and and animal status, for airway disease, vascular disease, parenchymal pneumonia, diffuse alveolar damage, eosinophils, and immunohistochemistry on a scale of 0 to 3 where 0 = none, 1 = mild, 2 = moderate, and 3 = severe.

Flow Cytometry Analysis

Whole peripheral blood from each mouse strain was collected in EDTA and mononuclear cells (PBMCs) were purified using density gradient centrifugation over Ficoll-Paque PLUS (GE Healthcare Life Sciences, Piscataway, NJ). Mouse lung tissues were first mechanically dissociated using scalpel blades then further digested using type A collagenase (Worthington Biochemical, Lakewood, NJ) in media prepared with DNase I (1mg/ml) for 1 hour in a shaking incubator at 37°C. Digested lung suspensions were filtered, centrifuged and treated with ACK lysis buffer. Single cell suspensions from blood and lung tissue were resuspended at 1×10^7 cells/ml in RPMI 1640 media supplemented with 10% heat-inactivated FBS and antibiotic/antimycotic cocktail (all Gibco), and were used immediately for flow cytometry. Single cell suspensions were plated in 200μl volumes per well on 96-well, round-bottom plates and stained for flow cytometry using the Intracellular Fixation and Permeabilization Buffer Set (eBioscience, San Diego, CA) according to the manufacturer's protocol and antibodies specific for CD3 (clone 145-2C11), CD4 (clone GK1.5), CD8 (clone 53-6.7; eBioscience), CD25 (clone PC61), CD26/DPP4 (clone H194-112; Biolegend, San Diego, CA), CD69 (clone H1.2F3; eBioscience), IFN-γ (clone XMG1.2), TNF-α (clone MP6-XT22; eBioscience), and IL-2 (clone JES6-5H4; eBioscience). All antibodies were purchased from BD Bioscience (San Jose, CA), unless indicated. Cells were also treated with a Fixable Live/Dead Discriminator (Invitrogen). Stained cells were fixed for 20 minutes in 1% PFA, resuspended in PBS and stored at 4°C before acquisition within 24 hours. Cell populations were first gated to exclude i) debris, ii) doublet events, and iii) dead cells before phenotypic and functional gating. All samples were stained in parallel with fluorescence minus one controls. A minimum of 100,000 live, singlet events were acquired per sample and data were analyzed using FlowJo software (TreeStar, Ashland, OR).

Northern Blot Analysis and RT-PCR

Northern blot analysis was performed for detection of full-length mouse DPP4 in the lungs of 288-330$^{+/+}$, 288-330$^{+/-}$, and C57Bl/6J wild-type mice. Poly (A) RNA was isolated to eliminate ribosomal RNA (Qiagen). Equivalent amounts of RNA were resolved on 0.8% agarose gels and transferred to nitrocellulose membrane. A biotinylated probe, 5′-[Btn]gATg[BtndT]gCTggTgAgCTgTgCTgCTAgCgATCCCgTggTCTTCATCC-3′, was used to detect mouse DPP4.

For quantifying viral and targeted host mRNAs, MERS-CoV, mouse DPP4, and mouse GAPDH RNAs were measured in brain and lung tissue from MERS-CoV-infected mice. Briefly, tissues were removed and placed into RNALater (Ambion) solution and stored at −80°C until analysis by RT-PCR. Lung tissue was homogenized in TRIzol reagent

(Invitrogen), and isolated according to manufacturer's instructions. Standard RT-PCR was performed with the following primer pairs for each of the indicated RNAs: MERS-CoV subgenomic transcript MERS leader 5′-CTATCTCACTTCCCCTCgTTCTC-3′ and 59R 5′-GAATCATTGTTAGGGTTCCG-3′; mGAPDH 5′-CAACgACCCCTTCATTgACC-3′ and mGAPDH 5′-gCAgggATgATgTTCTgggC-3′; and, mouse DPP4 5′-TAACgACACAggAgTgCCgC-3′ and mouse DPP4 5′-TCTgCTTTTTgACTACAggg-3′. Equivalent volumes of PCR product were resolved on the gels for a non-quantitative answer (presence or absence) of viral subgenomic transcript in the brain and lung.

Quantitative RT-PCR was executed on a Roche LightCycler 480 II, with accompanying software, to analyze MERS-CoV viral RNA, mDPP4 mRNAs, and 18S ribosomal RNA as an endogenous control. All RNAs were reverse transcribed under standard conditions in a 20μl reaction volume using SuperScript III reverse transcriptase (Invitrogen). MERS-CoV viral RNA was assessed using 900nM of the following primers in a 20μl reaction with SyBr Green assay with 2X SsoAdvanced Universal SYBR Green Supermix (Biorad). The forward primer anneals at the MERS-CoV leader sequence in the 5′ UTR (5′-GAATAGCTTGGCTATCTCAC-3′) and reverse primer anneals in the N gene (5′-TTGTTATCGGCAAAGGAAAC-3′). PCR conditions were 45 cycles of 95°C/10sec, 59°C/10sec, and 72°C/15sec. Standard Taqman conditions were used to analyze expression of mDPP4 and 18S ribosomal RNAs. The following primers and probe were used for mDPP4: Forward primer (5′-CCCCAAGACAGTGTGGATTC-3′); reverse primer (5′-GAGGATGAGCTGAGAGAGTCTATATTT-3′); and probe #51 was used from the Roche Universal ProbeLibrary. PCR conditions were 45 cycles of 95°C/15sec and 60°C/50sec. A 20X commercially available primer-probe set was utilized to quantitate the 18S ribosomal RNA (Life Technologies).

Statistical analysis

All quantitative data are presented as averages ± one standard deviation (SD). Significance between specific data sets is described in the respective figure legend and was determined using the student *t*-test function using a one-tailed or two-tailed distribution in Microsoft Excel software.

Biosafety and biosecurity

In vivo adaptation of the MERS-0 virus in mice had been executed prior to the US Government Deliberative Process Research Funding Pause on Selected Gain-of-Function Research Involving Influenza, MERS and SARS viruses http://www.phe.gov/s3/dualuse/Documents/gain-of-function.pdf). When notice to cease all *in vivo* passage experiments was received, all studies to adapt the MERS-0 virus *in vivo* where immediately halted. Following our formal written request for continuation, and then receiving an exemption from the pause and approval to continue after NIAID/NIH review, the *in vivo* adaptation of MERS-0 was then continued by serial passage in mice. All studies comprising the use of MERS-CoV where executed in BSL3 facilities at UNC-CH, under conditions described previously[35].

The following biosafety and biosecurity paragraph is as described by Menachery *et al.*[35]. All work for these studies was performed with approved standard operating procedures (SOPs)

and safety conditions for MERS-CoV (not a select agent), SARS-CoV (select agent), and derivatives therein. Our institutional CoV BSL3 facilities have been designed to conform to the safety requirements that are recommended in the Biosafety in Microbiological and Biomedical Laboratories (BMBL), the US Department of Health and Human Services, the Public Health Service, the Centers for Disease Control (CDC) and the NIH. Laboratory safety plans were submitted to, and the facility has been approved for use by, the UNC Department of Environmental Health and Safety (EHS) and the CDC. Electronic card access is required for entry into the facility. All workers have been trained by EHS to safely use powered air purifying respirators (PAPRs), and appropriate work habits in a BSL3 facility and active medical surveillance plans are in place. Our BSL3 facilities contain redundant fans, emergency power to fans and biological safety cabinets and freezers, and our facilities can accommodate SealSafe mouse racks. Materials classified as BSL3 agents consist of MERS-CoV, SARS-CoV, bat CoV precursor strains, and mutants derived from these pathogens. Within the BSL3 facilities, experimentation with infectious virus is performed in a certified Class II Biosafety Cabinet (BSC). All members of the staff wear scrubs, Tyvek suits and aprons, PAPRs and shoe covers, and their hands are double-gloved. BSL3 users are subject to a medical surveillance plan monitored by the University Employee Occupational Health Clinic (UEOHC), which includes a yearly physical, annual influenza vaccination and mandatory reporting of any symptoms associated with CoV infection during periods when working in the BSL3. All BSL3 users are trained in exposure management and reporting protocols, are prepared to self-quarantine and have been trained for safe delivery to a local infectious disease management department in an emergency situation. All potential exposure events are reported and investigated by EHS and UEOHC, with reports filed to both the CDC and the NIH.

Data Availability

The data that support the findings of this study are available from the corresponding author upon request.

Supplementary Material

Refer to Web version on PubMed Central for supplementary material.

Acknowledgments

The studies presented here were supported by grants from the National Institute of Allergy & Infectious Disease of the US National Institutes of Health (NIH) by awards HHSN272201000019I-HHSN27200003 (R.S.B. and M.T.H.), AI106772, AI108197, AI110700 and AI109761 (R.S.B.), and U19 AI100625 (R.S.B. and M.T.H.). Gain of Function research considerations involving MERS-0 *in vivo* passage in mice and the current manuscript were both reviewed and approved by the funding agency, the National Institutes of Health (NIH). The content is solely the responsibility of the authors and does not necessarily represent the official views of the NIH. Generation of CRISPR/Cas9 modified mice was performed at the UNC Animal Models Core Facility under the direction of Dr. Dale Cowley.

References

1. Chan JF, et al. Treatment With Lopinavir/Ritonavir or Interferon-beta1b Improves Outcome of MERS-CoV Infection in a Nonhuman Primate Model of Common Marmoset. The Journal of infectious diseases. 2015; 212:1904–1913. [PubMed: 26198719]

2. de Wit E, et al. Middle East respiratory syndrome coronavirus (MERS-CoV) causes transient lower respiratory tract infection in rhesus macaques. Proc Natl Acad Sci U S A. 2013; 110:16598–16603. [PubMed: 24062443]

3. Falzarano D, et al. Infection with MERS-CoV causes lethal pneumonia in the common marmoset. PLoS Pathog. 2014; 10:e1004250. [PubMed: 25144235]

4. Munster VJ, de Wit E, Feldmann H. Pneumonia from human coronavirus in a macaque model. The New England journal of medicine. 2013; 368:1560–1562.

5. Johnson RF, et al. 3B11-N, a monoclonal antibody against MERS-CoV, reduces lung pathology in rhesus monkeys following intratracheal inoculation of MERS-CoV Jordan-n3/2012. Virology. 2016; 490:49–58. [PubMed: 26828465]

6. Johnson RF, et al. Intratracheal exposure of common marmosets to MERS-CoV Jordan-n3/2012 or MERS-CoV EMC/2012 isolates does not result in lethal disease. Virology. 2015; 485:422–430. [PubMed: 26342468]

7. Cockrell AS, et al. Mouse dipeptidyl peptidase 4 is not a functional receptor for Middle East respiratory syndrome coronavirus infection. J Virol. 2014; 88:5195–5199. [PubMed: 24574399]

8. Coleman CM, Matthews KL, Goicochea L, Frieman MB. Wild-type and innate immune-deficient mice are not susceptible to the Middle East respiratory syndrome coronavirus. J Gen Virol. 2014; 95:408–412. [PubMed: 24197535]

9. de Wit E, et al. The Middle East respiratory syndrome coronavirus (MERS-CoV) does not replicate in Syrian hamsters. PLoS One. 2013; 8:e69127. [PubMed: 23844250]

10. Raj VS, et al. Adenosine deaminase acts as a natural antagonist for dipeptidyl peptidase 4-mediated entry of the Middle East respiratory syndrome coronavirus. J Virol. 2014; 88:1834–1838. [PubMed: 24257613]

11. Ohnuma K, Dang NH, Morimoto C. Revisiting an old acquaintance: CD26 and its molecular mechanisms in T cell function. Trends Immunol. 2008; 29:295–301. [PubMed: 18456553]

12. Agrawal AS, et al. Generation of a transgenic mouse model of Middle East respiratory syndrome coronavirus infection and disease. J Virol. 2015; 89:3659–3670. [PubMed: 25589660]

13. Li K, et al. Middle East Respiratory Syndrome Coronavirus Causes Multiple Organ Damage and Lethal Disease in Mice Transgenic for Human Dipeptidyl Peptidase 4. The Journal of infectious diseases. 2016; 213:712–722. [PubMed: 26486634]

14. Zhao G, et al. Multi-Organ Damage in Human Dipeptidyl Peptidase 4 Transgenic Mice Infected with Middle East Respiratory Syndrome-Coronavirus. PLoS One. 2015; 10:e0145561. [PubMed: 26701103]

15. Zhao J, et al. Rapid generation of a mouse model for Middle East respiratory syndrome. Proc Natl Acad Sci U S A. 2014; 111:4970–4975. [PubMed: 24599590]

16. Lambeir AM, Durinx C, Scharpe S, De Meester I. Dipeptidyl-peptidase IV from bench to bedside: an update on structural properties, functions, and clinical aspects of the enzyme DPP IV. Crit Rev Clin Lab Sci. 2003; 40:209–294. [PubMed: 12892317]

17. Menachery VD, Gralinski LE, Baric RS, Ferris MT. New Metrics for Evaluating Viral Respiratory Pathogenesis. PLoS One. 2015; 10:e0131451. [PubMed: 26115403]

18. Ng DL, et al. Clinicopathologic, Immunohistochemical, and Ultrastructural Findings of a Fatal Case of Middle East Respiratory Syndrome Coronavirus Infection in the United Arab Emirates, April 2014. Am J Pathol. 2016; 186:652–658. [PubMed: 26857507]

19. Tang XC, et al. Identification of human neutralizing antibodies against MERS-CoV and their role in virus adaptive evolution. Proc Natl Acad Sci U S A. 2014; 111:E2018–2026. [PubMed: 24778221]

20. Agnihothram S, et al. A mouse model for Betacoronavirus subgroup 2c using a bat coronavirus strain HKU5 variant. mBio. 2014; 5:e00047–00014. [PubMed: 24667706]

21. Korteweg C, Gu J. Pathology, molecular biology, and pathogenesis of avian influenza A (H5N1) infection in humans. Am J Pathol. 2008; 172:1155–1170. [PubMed: 18403604]

22. Ng WF, To KF, Lam WW, Ng TK, Lee KC. The comparative pathology of severe acute respiratory syndrome and avian influenza A subtype H5N1–a review. Human pathology. 2006; 37:381–390. [PubMed: 16564911]

23. Sanders CJ, et al. Compromised respiratory function in lethal influenza infection is characterized by the depletion of type I alveolar epithelial cells beyond threshold levels. Am J Physiol Lung Cell Mol Physiol. 2013; 304:L481–488. [PubMed: 23355384]
24. Pascal KE, et al. Pre- and postexposure efficacy of fully human antibodies against Spike protein in a novel humanized mouse model of MERS-CoV infection. Proc Natl Acad Sci U S A. 2015; 112:8738–8743. [PubMed: 26124093]
25. Frieman M, et al. Molecular determinants of severe acute respiratory syndrome coronavirus pathogenesis and virulence in young and aged mouse models of human disease. J Virol. 2012; 86:884–897. [PubMed: 22072787]
26. Thornbrough JM, et al. Middle East Respiratory Syndrome Coronavirus NS4b Protein Inhibits Host RNase L Activation. mBio. 2016; 7:e00258. [PubMed: 27025250]
27. Dediego ML, et al. Pathogenicity of severe acute respiratory coronavirus deletion mutants in hACE-2 transgenic mice. Virology. 2008; 376:379–389. [PubMed: 18452964]
28. Sims AC, et al. Release of severe acute respiratory syndrome coronavirus nuclear import block enhances host transcription in human lung cells. J Virol. 2013; 87:3885–3902. [PubMed: 23365422]
29. Agrawal AS, et al. Passive Transfer of A Germline-like Neutralizing Human Monoclonal Antibody Protects Transgenic Mice Against Lethal Middle East Respiratory Syndrome Coronavirus Infection. Sci Rep. 2016; 6:31629. [PubMed: 27538452]
30. Laksitorini M, Prasasty VD, Kiptoo PK, Siahaan TJ. Pathways and progress in improving drug delivery through the intestinal mucosa and blood-brain barriers. Ther Deliv. 2014; 5:1143–1163. [PubMed: 25418271]
31. McCray PB Jr, et al. Lethal infection of K18-hACE2 mice infected with severe acute respiratory syndrome coronavirus. J Virol. 2007; 81:813–821. [PubMed: 17079315]
32. Lamers MM, et al. Deletion Variants of Middle East Respiratory Syndrome Coronavirus from Humans, Jordan, 2015. Emerg Infect Dis. 2016; 22:716–719. [PubMed: 26981770]
33. Scobey T, et al. Reverse genetics with a full-length infectious cDNA of the Middle East respiratory syndrome coronavirus. Proc Natl Acad Sci U S A. 2013; 110:16157–16162. [PubMed: 24043791]
34. Mali P, et al. RNA-guided human genome engineering via Cas9. Science (New York, NY). 2013; 339:823–826.
35. Menachery VD, et al. A SARS-like cluster of circulating bat coronaviruses shows potential for human emergence. Nat Med. 2015; 21:1508–1513. [PubMed: 26552008]
36. Ayala JE, et al. Standard operating procedures for describing and performing metabolic tests of glucose homeostasis in mice. Disease models & mechanisms. 2010; 3:525–534. [PubMed: 20713647]

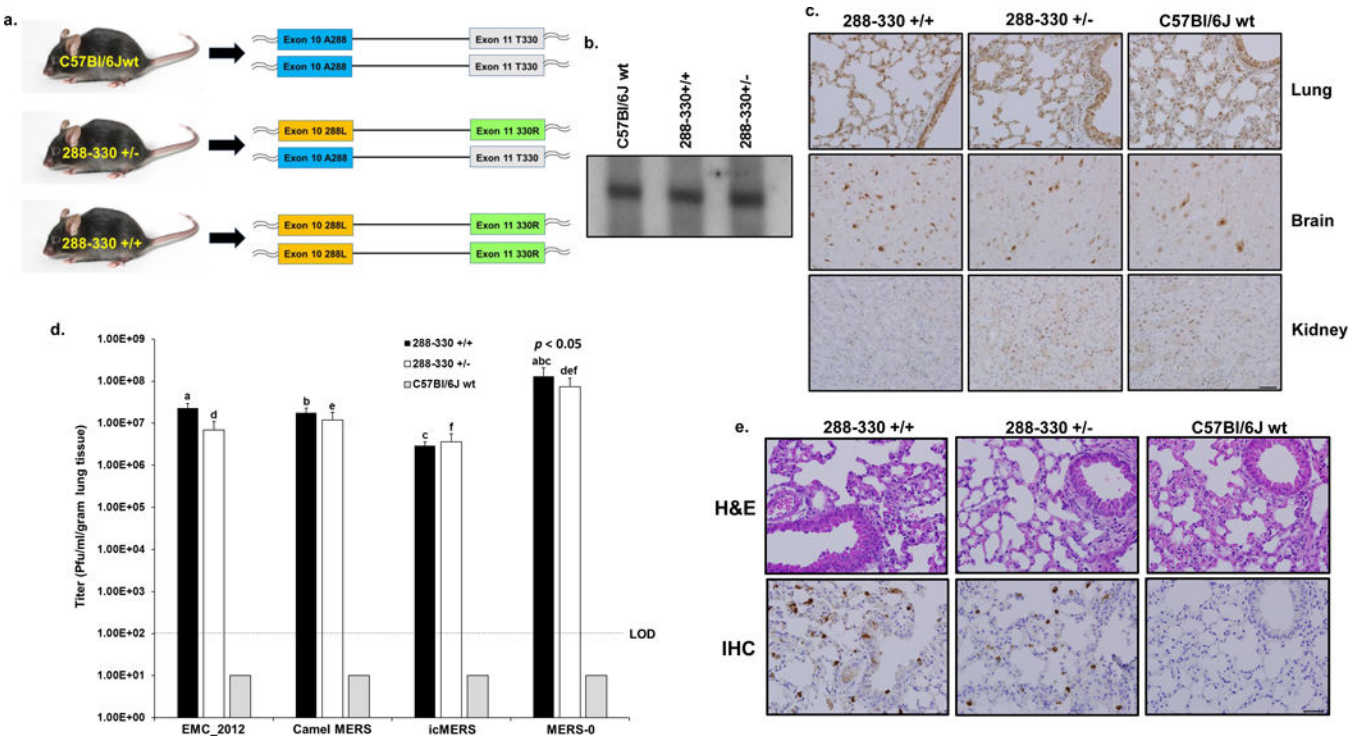

Figure 1.

A CRISPR/Cas9 genetically engineered mouse model for MERS-CoV replication. (a) CRISPR/Cas9 genetically engineered C57Bl/6J mice to encode 288L & 330R on mDPP4 of one chromosome (heterozygous, 288-330$^{+/-}$) and 288L & 330R on both chromosomes (homozygous, 288-330$^{+/+}$). (b) Northern blot of mDPP4 mRNA expression. (c) Immunohistochemistry (IHC) of mDPP4 protein in the lungs, brain, and kidneys of individual C57Bl/6J wild-type, 288-330$^{+/-}$, and 288-330$^{+/+}$ mice. (d) Viral titers for MERS-CoV at 3 days p.i. from C57Bl/6J wild-type (n = 4), 288-330$^{+/-}$ (n = 4), and 288-330$^{+/+}$ (n = 4) mice infected with the indicated viruses at 5×10^5 PFU. Bar graphs are averages +SD. Student t-test was used to calculate $p < 0.05$ for comparisons of MERS-0 with each virus in 288-330$^{+/+}$ mice (a, b, c) and 288-330$^{+/-}$ mice (d, e, f). (e) Pathology of 288-330$^{+/+}$, 288-330$^{+/-}$, and C57Bl/6J wild-type mice at 3 days p.i. with MERS-0. Lung tissue sections were stained to examine pathology by H&E, or stained by IHC to detect nucleocapsid protein from MERS-0 infection. IHC and H&E pathology images are representative of at least 3 samples. Scale bars in lower right panels are 1mm.

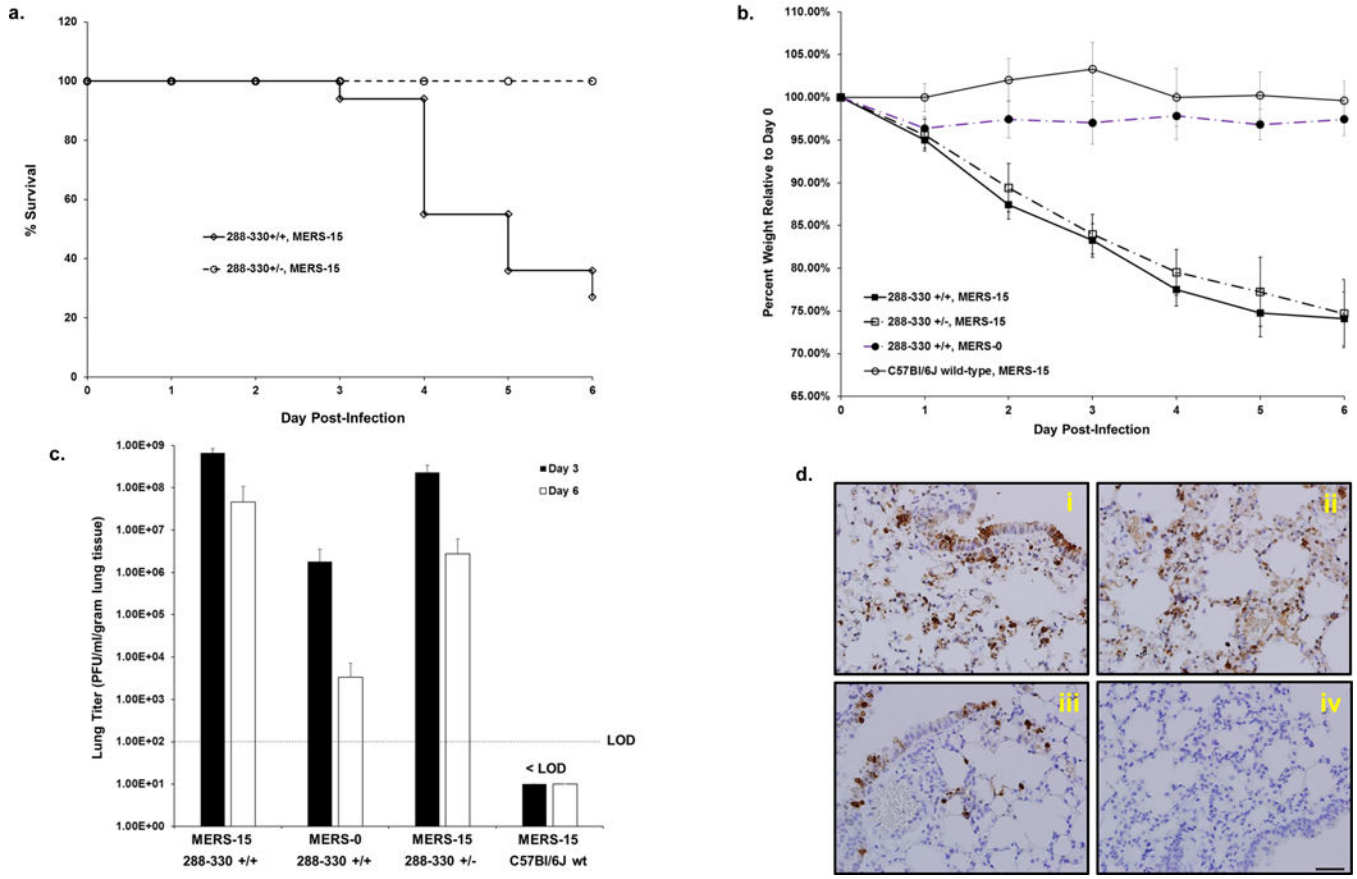

Figure 2.

Mouse adapted MERS-CoV causes fatal disease in 288-330$^{+/+}$ mice. Mice were inoculated intranasally with 5×10^{6} PFU. (a) Mortality of 288-330$^{+/-}$ (n = 10) and 288-330$^{+/+}$ (n = 16) mice was monitored daily through day 6 post-infection. Data reflect percent of surviving mice. (b) Mouse weights were measured daily through day 6 post-infection for 288-330$^{+/+}$ + MERS-15 (n = 16); 288-330$^{+/-}$ + MERS-15 (n = 10), 288-330$^{+/+}$ + MERS-0 (n = 10), and C57Bl/6J wt + MERS-15 (n = 7). Data are daily averages of the percent weight relative to day 0 ±SD. (c) Viral lung titers for MERS-CoV were determined at day 3 (n = 4 for 288-330$^{+/-}$ + MERS-15; n = 5 for 288-330$^{+/+}$ + MERS-15; n = 5 for 288-330$^{+/+}$ + MERS-0; n = 4 for C57Bl/6J wt + MERS-15) and day 6 (n = 4 for 288-330$^{+/-}$ + MERS-15; n = 4 for 288-330$^{+/+}$ + MERS-15; n = 5 for 288-330$^{+/+}$ + MERS-0; n = 3 for C57Bl/6J wt + MERS-15) post-infection. The limit of detection (LOD) is indicated. Bars are averages +SD. (d) Immunohistochemistry of lung sections for anti-MERS nucleocapsid at 3 days post-infection. 288-330$^{+/+}$ + MERS-15 (i); 288-330$^{+/-}$ + MERS-15 (ii); 288-330$^{+/+}$ + MERS-0 (iii); and C57Bl/6J wt + MERS-15 (iv). IHC images are representative of at least 3 samples. Scale bars in lower right panels are 1mm.

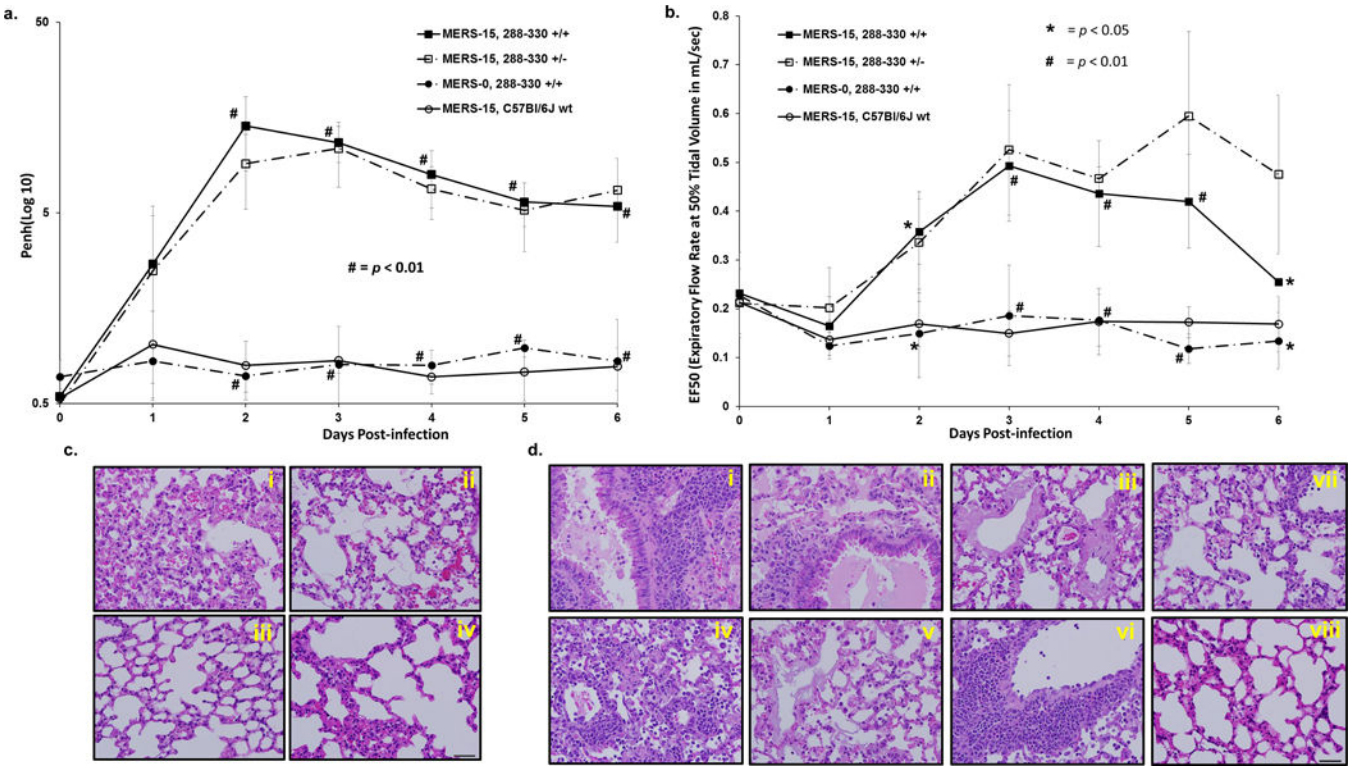

Figure 3.

Lung function in MERS-15-infected mice. Respiratory function was monitored in live mice through day 6 p.i. using whole-body plethysmography to measure enhanced pause (Penh) (a) and the expiratory flow rate at 50% tidal volume (EF50) (b) in 288-330$^{+/+}$ + MERS-15 (n = 9); 288-330$^{+/-}$ + MERS-15 (n = 4), 288-330$^{+/+}$ + MERS-0 (n = 3), and C57Bl/6J wt + MERS-15 (n = 3). Data are daily averages ±SD. Student t-test was used to compare 288-330$^{+/+}$ mice infected with MERS-15 and MERS-0, # is $p < 0.01$ and * is $p < 0.05$. (c) Pathology of lungs from infected mice at day 3 p.i. demonstrate severe inflammation for 288-330$^{+/+}$ (i) and 288-330$^{+/-}$ (ii) infected with MERS-15, and moderate inflammation for 288-330$^{+/+}$ + MERS-0 (iii) and C57Bl/6J wt + MERS-15 (iv). (d) Pathology at day 6 post-infection for 288-330$^{+/+}$ + MERS-15 images demonstrate severe inflammation and edema in large airways and alveoli (i) and (ii), and hyaline membrane formation (iii). 288-330$^{+/-}$ + MERS-15 exhibit severe inflammation throughout parenchyma (iv), hyaline membrane formation (v), and perivascular cuffing (vi). 288-330$^{+/+}$ + MERS-0 (vii) or C57Bl/6Jwt + MERS-15 (viii) exhibit mild-to-moderate inflammation. All images are at 40X magnification. H&E images are representative of at least 3 samples. Scale bars in lower right panels are 1mm.

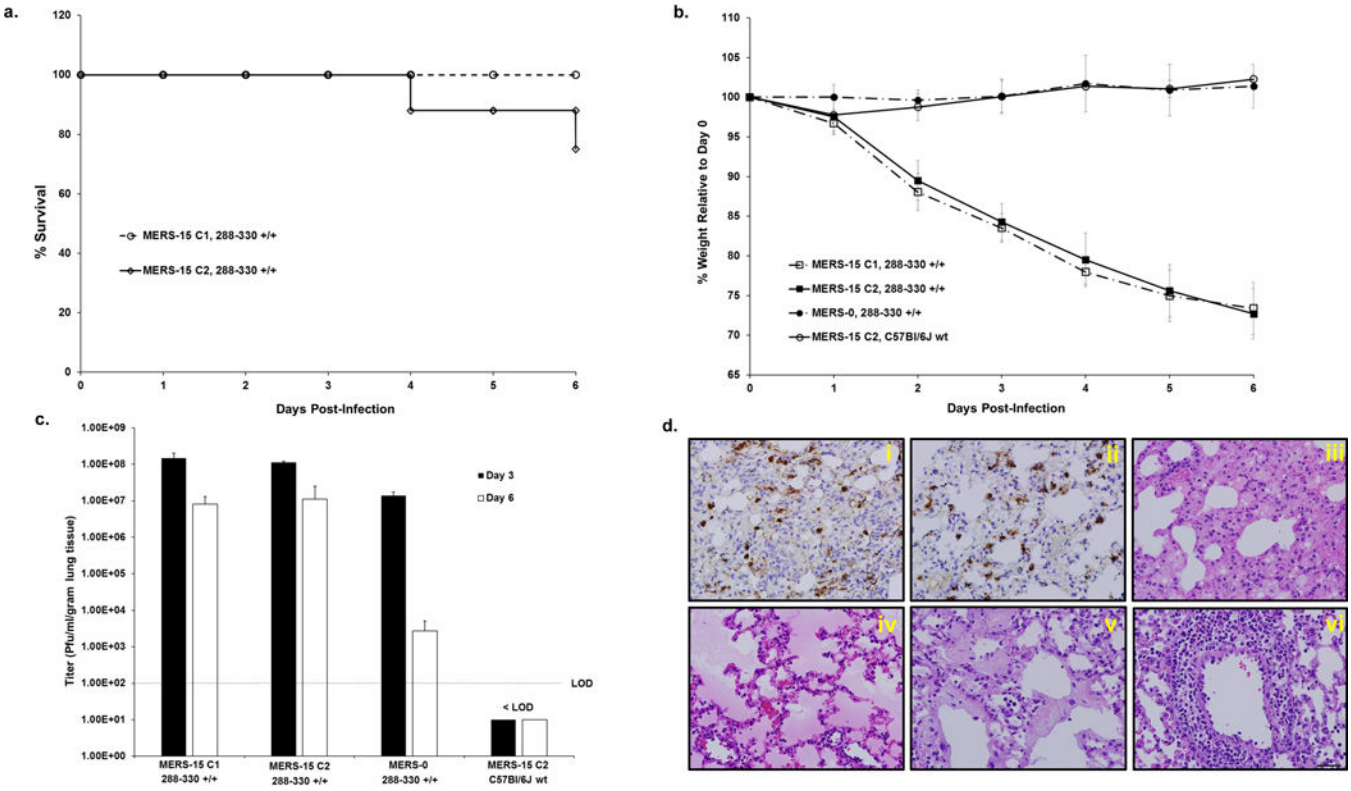

Figure 4.

Clonal isolates of mouse-adapted MERS-CoV exhibit severe respiratory disease. Mice were inoculated intranasally with 5×10^6 PFU. (a) Mortality of 288-330$^{+/+}$ + MERS-15 clone 1 (MERS-15 C1) (n = 7) or MERS-15 clone 2 (MERS-15 C2) (n = 11) was monitored daily through day 6 p.i. Data reflect percent of surviving mice. (b) Mouse weights were monitored daily for 288-330$^{+/+}$ + MERS-15 C1 (n = 7); 288-330$^{+/+}$ + MERS-15 C2 (n = 11); 288-330$^{+/+}$ + MERS-0 (n = 6); and C57Bl/6J wt + MERS-15 C2 (n = 6). Data are daily averages ±SD. (c) Viral lung titers were determined at day 3 (288-330$^{+/+}$ + MERS-15 C1, n = 4; 288-330$^{+/+}$ + MERS-15 C2, n = 3; 288-330$^{+/+}$ + MERS-0, n = 3; and C57Bl/6J wt + MERS-15 C2, n = 3) and day 6 (288-330$^{+/+}$ + MERS-15 C1, n = 4; 288-330$^{+/+}$ + MERS-15 C2, n = 6; 288-330$^{+/+}$ + MERS-0, n = 3; and C57Bl/6J wt + MERS-15 C2, n = 3). The limit of detection (LOD) is indicated. Bar graphs are averages +SD. (d) IHC of lung sections at 3 days p.i. from 288-330$^{+/+}$ + MERS-15 C1 (i) or MERS-15 C2 (ii) stained for nucleopcapsid. Pathology of lungs from 288-330$^{+/+}$ + MERS-15 C2 was assessed by H&E at day 6 p.i. Images demonstrate severe inflammation (iii), edema (iv), hyaline membrane formation (v), and perivascular cuffing (vi). Images are at 40X magnification. All H&E images are representative of at least 3 samples. Scale bar in lower right panel is 1mm.

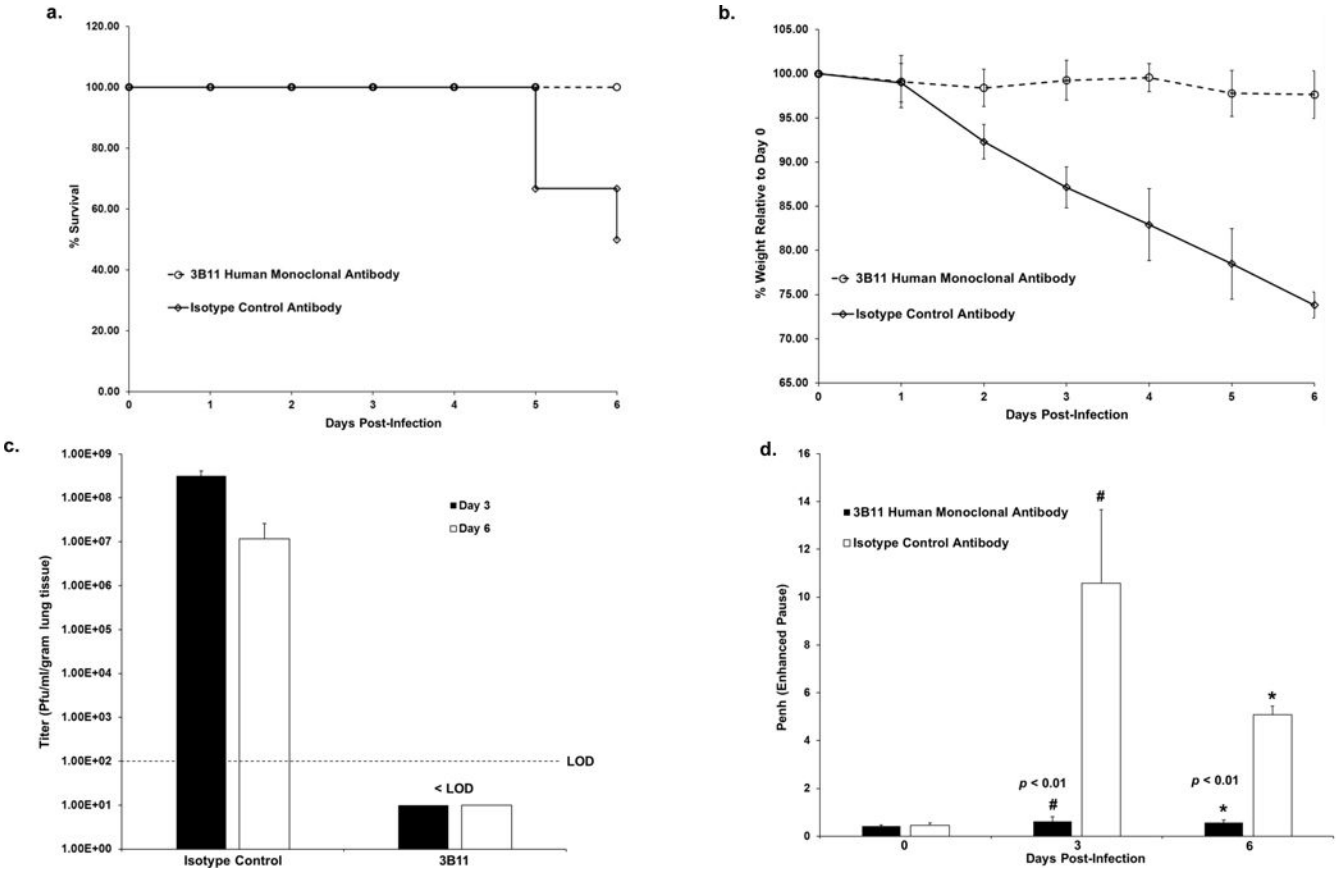

Figure 5.

Human monoclonal antibody, 3B11, protects mice from severe respiratory disease. 288-330$^{+/+}$ mice were intraperitoneally administered 250ug of 3B11 or isotype control antibody 12 hours prior to challenge with 5×10^6 PFU of MERS-15 C2. Mortality (a) and mouse weights (b) were monitored daily for mice receiving 3B11 human monoclonal antibody (n = 12) or isotype control antibody (n = 12) through day 6 p.i. Data reflect percent surviving mice (a) or daily weight averages ±SD (b). (c) Viral lung titers were determined at day 3 (n = 6 for each of 3B11 and isotype control antibody treated mice) and day 6 (n = 6 for 3B11 treated mice; n = 3 for isotype control antibody treated mice). The limit of detection (LOD) is indicated. Bar graphs are averages +SD. (d) Lung function was assessed by Penh (enhanced pause) at 0, 3, and 6 days p.i. for mice receiving 3B11 (n = 6 at days 0, 3, and 6) or isotype control (n = 6 at days 0 and 3, and n = 3 at day 6). Data are averages +SD. Student t-test was used to compare mice receiving 3B11 human monoclonal antibody with the isotype control antibody at day 3 (# is $p < 0.01$) and day 6 (* is $p < 0.01$) p.i.

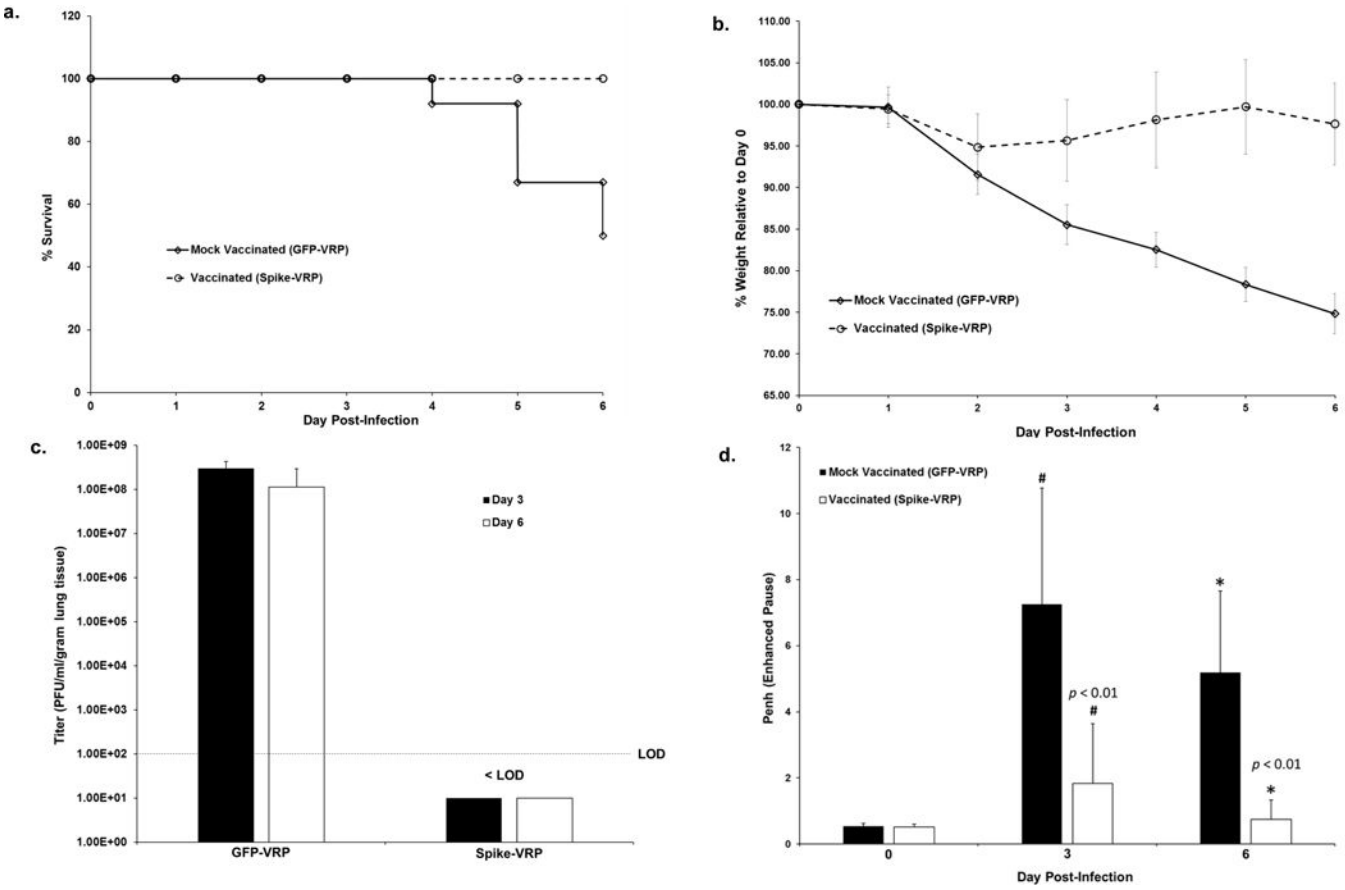

Figure 6.

Vaccination of 288-330$^{+/+}$ mice with a VRP delivering MERS-CoV spike protein protects mice from challenge with MERS-CoV. The vaccination protocol is described in methods. After a 5×10^{6} PFU challenge, mortality (a) and mouse weights (b) were monitored daily for mice receiving GFP-VRP (n = 19) or Spike-VRP (n = 19) through day 6 p.i. Data reflect percent survival (a) or daily weight averages ±SD (b). (c) Viral lung titers were determined day 3 (n = 7 for Spike-VRP and GFP-VRP) and day 6 (n = 12 for Spike-VRP; n = 6 for GFP-VRP) p.i. The limit of detection (LOD) is indicated. Bar graphs are averages +SD. (d) Lung function was assessed by Penh (enhanced pause) at 0, 3, and 6 days p.i. for mice receiving either GFP-VRP (n = 12 at days 0 and 3 p.i.; n = 6 at day 6 p.i.) or Spike-VRP (n = 12 at all days post-infection). Data represent averages +SD. Student t-test was used to compare mice receiving GFP-VRP with Spike-VRP vaccines at day 3 (# is $p < 0.01$) and day 6 (* is $p < 0.01$) p.i.